THE JOURNAL OF PROSTHETIC DENTISTRY

RESEARCH AND EDUCATION

Architecture and design of a robotic mastication simulator for interactive load testing of dental implants and the mandible

Ahmad Mahmood Tahir, PhD,[a] Michal Jilich, PhD,[b] Duc Cuong Trinh, PhD,[b] Giorgio Cannata, MS,[c] Fabrizio Barberis, PhD,[d] and Matteo Zoppi, PhD[e]

ABSTRACT

Statement of problem. Determination of interactive loading between a dental prosthesis and the host mandible is essential for implant prosthodontics and to preserve bone.

Purpose. The purpose of this study was to develop and evaluate a robotic mastication simulator to replicate the human mastication force cycle to record the required interactive loading using specifically designed force sensors.

Material and methods. This robotic mastication simulator incorporated a Stewart parallel kinematic mechanism (PKM) controlled in the force-control loop. The hydraulically operated PKM executed the wrench operation, which consisted of the combined effect of forces and moments exhibited by the mastication process. Principal design features of this robotic simulator included PKM kinematic modeling, static force analysis to realize the masticatory wrench characteristics, and the architecture of its hydraulic system. Additionally, the design of a load-sensing element for the mandible and implant interaction was also incorporated. This element facilitated the quantification of the load distribution between implants and the host bone during the masticatory operation produced by the PKM. These loading tests were patient-specific and required separate artificial mandibular models for each patient.

Results. The simulation results demonstrated that the robotic PKM could replicate human mastication. These results validated the hydraulic system modeling for the required range of masticatory movements and effective forces of the PKM end-effector. The overall structural design of the robotic mastication simulator presented the integration of the PKM and its hydraulic system with the premeditated load-recording mechanism.

Conclusions. The developed system facilitated the teeth-replacement procedure. The PKM accomplished the execution of mastication cycle involving 6 degrees of freedom, enabling any translation and rotation in sagittal, horizontal, and vertical planes. The mechanism can simulate the human mastication cycle and has a force application range of up to 2000 N. The designed load-sensing element can record interactive forces within the range of 200 N to 2000 N with fast response and high sensitivity to produce a robotic mastication simulator with custom-made modules. (J Prosthet Dent 2019;122:389.e1-e8)

Robotics technology in the medical field is one of the 6 major application areas of service robotics,[1] a trend, particularly in patient health care, that has been increasing since the 1980s[2,3] and especially during the last decade.[4,5] However, despite the accessibility of high-technology tools, the use of robotics in medical processes is still limited because of the cost, safety requirements, and system complexities.[6-8] The presence of robotics technology in dental care is even scarcer.[9]

Dental implants are important in various aspects of oral health.[10] Although implants might not be actively helpful in preserving the host mandible, they directly interact with the bone,[11] and their success depends on proper placement in the alveolar bone in addition to their design and composition.[12,13] Compromised alveolar bone requires clinical evaluation, as strength plays an important role in the success of an implant.[14-16] Such evaluations are generally performed through imaging technology or indentation and bending stiffness of implants after their placement.[17,18] These evaluations, along with preceding statistical data analyses of implant success rates,

[a]Research Scientist, Mechanics, Measurements and Robotics (MMR), DIME–PMAR Robotics Group, University of Genoa, Genoa, Italy.
[b]Research Scientist, DIME–PMAR Robotics Group, University of Genoa, Genoa, Italy.
[c]Associate Professor, The Department of Informatics, Bioengineering, Robotics and Systems Engineering (DIBRIS), University of Genoa, Genoa, Italy.
[d]Associate Professor, The Department of Civil, Chemical and Environmental Engineering (DICCA), University of Genoa, Genoa, Italy.
[e]Associate Professor, DIME–PMAR Robotics Group, University of Genoa, Genova, Italy.

Clinical Implications

The robotic mastication simulator, with its innovative design and optimized structural components, may facilitate the optimal placement of dental implants.

help place an implant appropriately. However, a system to assess the strength of bone quantitatively before implant placement is lacking.[19]

Patient-specific evaluation is considered essential for this procedure because of 2 distinctive aspects: the periodontal ligament (PDL) and the alveolar bone structure. The PDL attachment to natural teeth disseminates isotropic forces inside the bone but is lost upon tooth removal. In the absence of a PDL, implants exert a larger linear vertical force to the bone,[20] with loading from implants increasing the risk of bony fracture.[21,22] The relationship of the maxilla to the mandible is unique to every patient[23] as is the relationship with the temporomandibular joints, making jaw movements and resultant forces distinctive for every individual.

Robotic mastication systems have been developed for rehabilitation, food sciences, and dental implant testing,[24] with a focus on reproducing the biomechanics of human mastication. A mastication system was developed for temporomandibular joint disorders and open anterior relationship malocclusion. Initially, it was a single degree of freedom (Dof) antagonistic muscle model that was modified into a 3-Dof masticatory robot and then reconfigured into a 6-Dof mechanism for maximum dexterity,[25-29] with the aim of replicating the mechanical structure, Dof, and sensing capability of human mastication. The 6-Dof version was further used for food texture analysis.[29] Other robots used in the food sciences include a 6-Dof parallel manipulator, a 6-bar linkage robot, and a tendon-spring robotic mechanism.[30-34]

A biomimetic mastication robot with redundant kinematic structure, a commercial selective compliance assembly robot arm (SCARA), robot to execute occlusal forces, and a parallel kinematic mechanism (PKM) to simulate mastication forces have been reported for testing dental implant materials.[35-39] Industrial grade systems have also been developed to conduct monotonic and cyclic tests, which are predominately uniaxial compression and tensile testers.[40-43] These systems are also used for International Standards Organization (ISO) 14801 standardization testing.[44-46] The focus of all these systems is largely on mandibular biomechanics. Although, the motion capability of developed systems has ranged from single Dof to kinematic redundancy, force sensing is limited. Furthermore, their control systems have been based on position and velocity feedback, with the control loop deficient in force feedback. Lack of force feedback hinders the achievement of the required level of masticatory force cycle replication. An appropriate system for the effective implant-mandible interactive load examination is required.

To address this need, the present robotic system was developed to replicate the complex action of the mandible on the maxilla to replicate forces over a normal mastication cycle. The end-effector of the PKM acts as the mandible that interacts with a specially designed load-recording module fixed within the apparatus. The PKM executes wrench in 6 Dof—a translation and a rotation in each of sagittal, horizontal, and vertical planes. Maximum force is required in the horizontal plane or the occlusal direction, while lesser forces are required in other directions. Here, the focus was not on the end-effector manipulation but on wrench execution at a point of interest. Human occlusal forces are limited to 1200 N, with an average range of approximately 300 N to 600 N in the molar region.[47] An optimal level was

Table 1. Nomenclature and abbreviations used

Abbreviation	Description
PKM	Parallel kinematic mechanism—the robotic Stewart mechanism
b	Base of the PKM
p	End-effector of the PKM
A, B, C, D, E, F	Legs of the PKM
b1–b6	Vertices of the PKM legs on the base "b"
p1–p6	Vertices of the PKM legs on the end-effector "p"
$\vec{r}_{0b}$	Initial vector for vertices on base "b"
$\vec{r}_{0p}$	Initial vector vertices on end-effector "p"
Z	Axis of rotation for base and end-effector initial vectors $\vec{r}_{0b}$ and $\vec{r}_{0p}$
r_b	Radius of base vertices: b1 - b6
r_p	Radius of end-effector vertices: p1 - p6
θ_b	Angle between vertices on smaller side of base
θ_p	Angle between vertices on larger side of end-effector
α	Rotational symmetry angle for alternate pair of vertices on "b" and "p"
H	Height of the PKM
$I(\xi_n^L)$	Revolute or prismatic Dof, of the PKM
ξ	Twist for each leg of the PKM
ω_n^L	One revolute joint of the PKM
ρ_n^L	One prismatic joint of the PKM
φ^L	One screw, reciprocal to all the passive joint twists in respective leg
J	Kinematic Jacobian matrix of the robot
J_q	Dimensionless diagonal matrix for forces and translations of the robot
F	The vector of the generalized end-effector or Cartesian forces
$\mathscr{T}$	The vector of the articular forces
G	Point of interest on the end-effector for resultant forces
M	Parametric configuration of forces and moments of the PKM
W	The wrench (combined effect of forces and moments)
Ω	Capacitance of a mesh point of the load-recording sensor
a	Nominal area of a sensing patch of the load-recording sensor
χ	Sensing plates separation in a sensing patch of the load-recording sensor

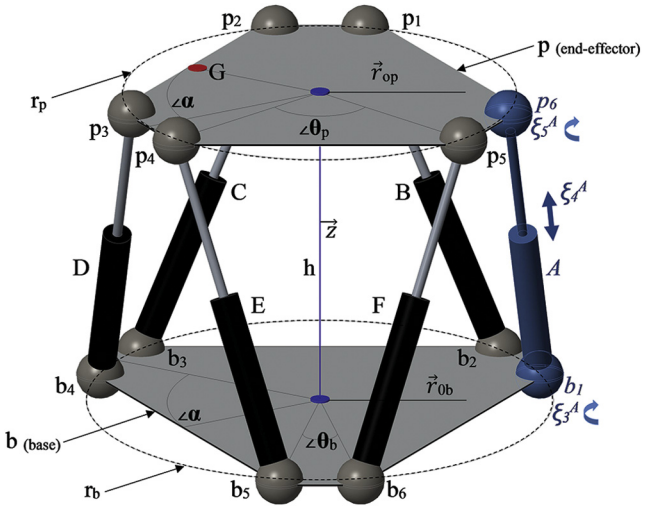

Figure 1. Geometry of PKM. Vertices b_1 to b_6 on base (b) and p_1 to p_6 on end-effector (p) from initial vectors $\vec{r}_{0b}$ and $\vec{r}_{0p}$, angle θ_p of pair of vertices on larger edges, angle θ_b of pair of vertices on smaller edges, rotational symmetry angle α, and kinematics of leg A. PKM, parallel kinematic mechanism.

achieved to conduct real-time tests. The apparatus has 3 main modules: the PKM, the hydraulic actuation system, and the dental implant module. These modules are integrated with respective control units and the power supply, focusing on compactness, structural stability, safety, and user-friendly operation. Design level optimization for the functional performance of the equipment has been accomplished. This approach further bridges the gap between academic research and industrial grade design for commercial application. The nomenclature used to describe the system design is listed in Table 1.

MATERIAL AND METHODS

The PKM used 6 identical linear hydraulic actuators as its legs, which were hinged to the base plate and the end-effector plate in 3 pairs of vertices distributed in a circle (Fig. 1). The radii of the vertices were 120 mm and 102 mm, and the height of the PKM was 165 mm with an extension stroke of 50 mm. At each hinge vertex, spherical floating joints were used to compensate for backlash in the mechanism to form a spherical-prismatic-spherical (SPS) kinematic chain for each leg. For kinematic modeling, a spherical joint was composed of 3 revolute joints, commonly perpendicular and intersecting each other. For instance, for leg A, which was hinged at b_1 and p_6 vertices, 3 revolute joints at b_1 were represented as $l(\xi_1^L) \perp l(\xi_2^L) \perp l(\xi_3^L)$ which implied $P_1^L \equiv P_2^L \equiv P_3^L$, and 3 revolute joints at p_6 were represented as $l(\xi_5^L) \perp l(\xi_6^L) \perp l(\xi_7^L)$ which implied $P_5^L \equiv P_6^L \equiv P_7^L$. The prismatic joint $l(\xi_4^A)$ of the leg A connected perpendicularly with $l(\xi_3^L)$ and $l(\xi_5^L)$ such that $l(\xi_3^L) \perp l(\xi_4^L) \perp l(\xi_5^L)$.

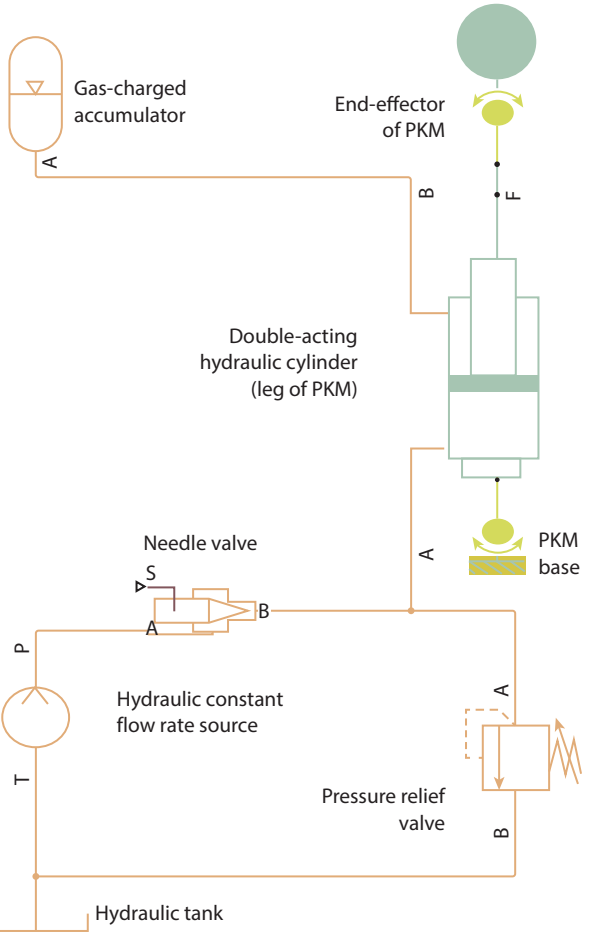

Figure 2. Hydraulic circuit for single leg of PKM. PKM, parallel kinematic mechanism.

Calculation of the wrench being applied to the end-effector by the actuators was necessary to determine the extreme values of articular forces for proper actuators and passive joint selection. Conversely, limited specifications of actuators and passive joints were required to determine corresponding maximal Cartesian forces. A static analysis was performed to determine these relationships in a static equilibrium state. The methods used, the screw theory and virtual work principle, furnished the calculation of actuator forces as a function of externally applied forces or vice versa, eliminating the need to discover internal reactions in the mechanism. To derive the static equations of the PKM from its instantaneous kinematic ones, the transpose of its Jacobian was a matrix that correlated the end-effector wrench to the actuator torques and/or forces. Since the joints were spherical, the twist equation for each leg was driven out as $\xi = \omega_1^L \xi_1^L + \omega_2^L \xi_2^L + \omega_3^L \xi_3^L + \dot{d}_4^L \xi_4^L + \omega_5^L \xi_5^L + \omega_6^L \xi_6^L + \omega_7^L \xi_7^L$. Specifying the revolute and the prismatic joint as ρ_i^L and τ_4^L, respectively, the equation was modified as $\xi = \omega_1^L \rho_1^L + \omega_2^L \rho_2^L + \omega_3^L \rho_3^L + \dot{d}_4^L \tau_4^L + \omega_5^L \rho_5^L + \omega_6^L \rho_6^L + \omega_7^L \rho_7^L$. To simplify the

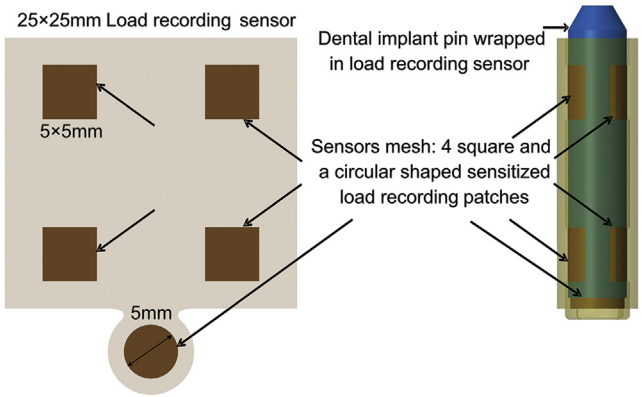

Figure 3. Force-sensing element with 5 patches: 4 square built-in sensing patches to wrap around dental implant for bending loads, and 1 bottom rounded patch for vertical load recording.

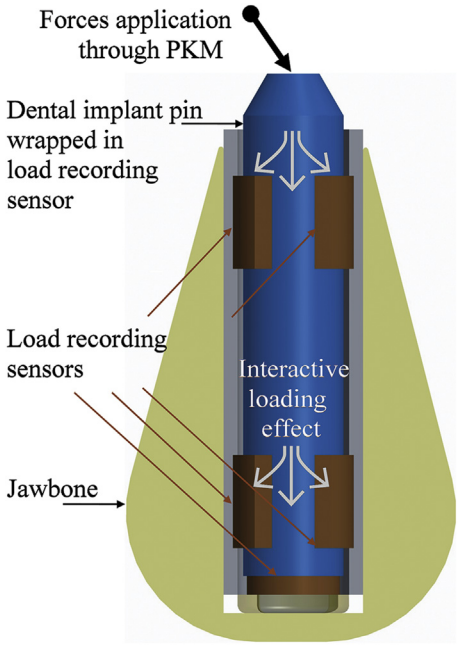

Figure 4. Side view of load-recording sensor module inside mandible: force-sensing element wrapped around metallic pin and inserted into hole of mandible model.

equation, a screw was chosen depending on passive joint screws in the leg. For revolute passive joints, the reciprocal screw was a zero-pitch screw (that is, a pure force) with an axis intersecting centers of all revolute passive joints in the chain. To eliminate passive joint velocities, each equation was multiplied with a screw which was reciprocal to all passive joint twists in the leg. So, 6 scalar equations were derived for 6 legs: $\phi^L \xi = \phi^L \tau_4^L \dot{d}_4^L$, where $L=A, B, C, D, E, F$. These equations were arranged in matrix form as $J_x \dot{x} = J_q \dot{q}$ and $J = J_x^{-1} J_q$, where J was the Jacobian of the robot that correlated the linear and angular velocities of the end-effector to the joint rates.

Elaborating the Jacobian further, $J_x = [\tilde{\varphi}^A \tilde{\varphi}^B \tilde{\varphi}^C \tilde{\varphi}^D \tilde{\varphi}^E \tilde{\varphi}^F]^T$ for which $\tilde{\varphi}^L = [r^L \times u^L u^L]^T$, where u^L was a unit vector along the line of action $l(\xi_4^L)$ and r^L was a position vector of u^L with respect to the base frame. The sign "$\sim$" on φ^L pointed out the direction and moment parts, which were swapped for the sake of manipulation between matrices. Now, $J_q = \text{diag}(\varphi_1\tau_1, \varphi_2\tau_2, \varphi_3\tau_3, \varphi_4\tau_4, \varphi_5\tau_5, \varphi_6\tau_6)$, which was a diagonal matrix with dimensionless entries because the forces φ^L and translations τ_4^L were unit screws with the same direction. Hence, $J_q = I_6$. The principle of the virtual work revealed that the Jacobian J correlated with the resultant force and torque applied by the end-effector to joint torques as $\mathcal{T} = J^T F$, where $\mathcal{T}$ was the vector of articular forces, F was the vector of a generalized end-effector or Cartesian forces, and J was the kinematic Jacobian matrix. This correlation indicated that $F = J^{-T} \mathcal{T}$, which specified that given the pose of the end-effector, the kinematic Jacobian matrix with the addition of the articular force can be calculated.

To realize the mastication wrench, an unconventional hydraulic actuation scheme was implemented in 2 stages: the initial extension stage of the end-effector to get engaged with the dental implant module, and the second stage where the end-effector executed the wrench. The implemented hydraulic circuit consisted of 6 double-acting hydraulic cylinders that were linked to a constant displacement hydraulic source from their bore sides and to a gas-charged hydraulic accumulator from the rod sides. Each hydraulic cylinder used a needle valve and a pressure-relief valve for hydraulic flow control. Hydraulic architecture for a single leg is presented in Figure 2. The hydraulic source kept the volumetric flow constant, with some losses based on the system pressure dynamics. The accumulator with a precharged pressure of 10 MPa was used. Manually operated needle valves were set to a fixed open state. An ideally controlled pressure-relief valve, whose losses were calculated to simulate the clinical situation, was used for each actuator. In the first stage, the hydraulic source delivered the flow to extend the end-effector toward the dental implant module. In the second stage, the hydraulic source maintained the required fluid supply against any pressure differential to ensure necessary forces at the end-effector.

The end-effector was equipped with a load cell for wrench feedback, and hydraulic cylinders were equipped with respective pressure sensors. Feedbacks from the load cell and pressure sensors were used to satisfy the relationship $MF=W$, where M was the parametric configuration, F was the force vector at the end-effector, and W was the wrench at the end-effector. The system was solved with regard to leg extensions to obtain a parametric configuration that accomplished the control of the hydraulic cylinders. The position sensing of the legs was not incorporated as the system was not a manipulator for peculiar pose identification, which reduced the complexity and cost of the system. System-level calibration had been

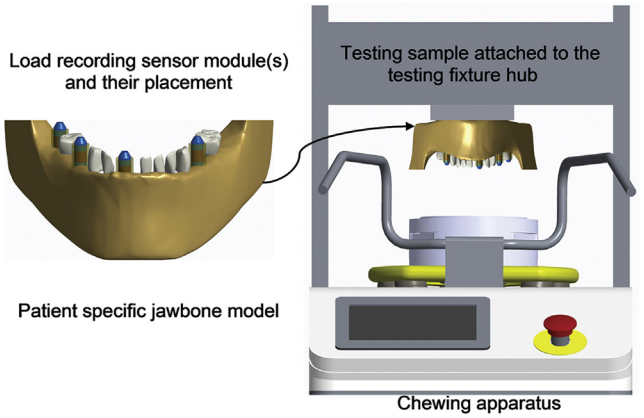

Figure 5. Test specimen preparation and fixture on robotic mastication simulator. Test model preparation and execution of interactive load-recording operation.

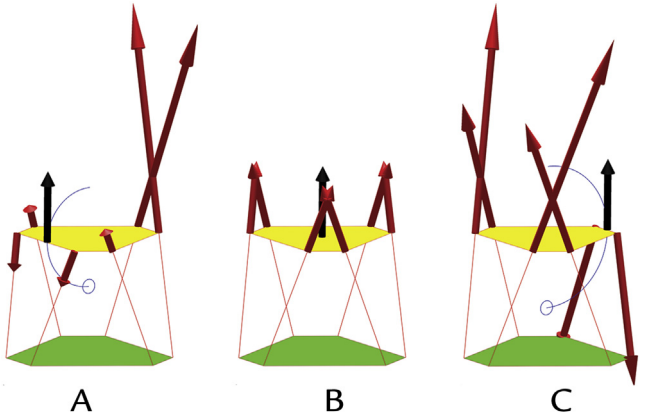

Figure 6. Wrench at point of interest G. Vertical arrow on end-effector (p) gives resultant force N and arc around it. A, C, Torque N.m. B, G at center of end-effector (p) (no torque case).

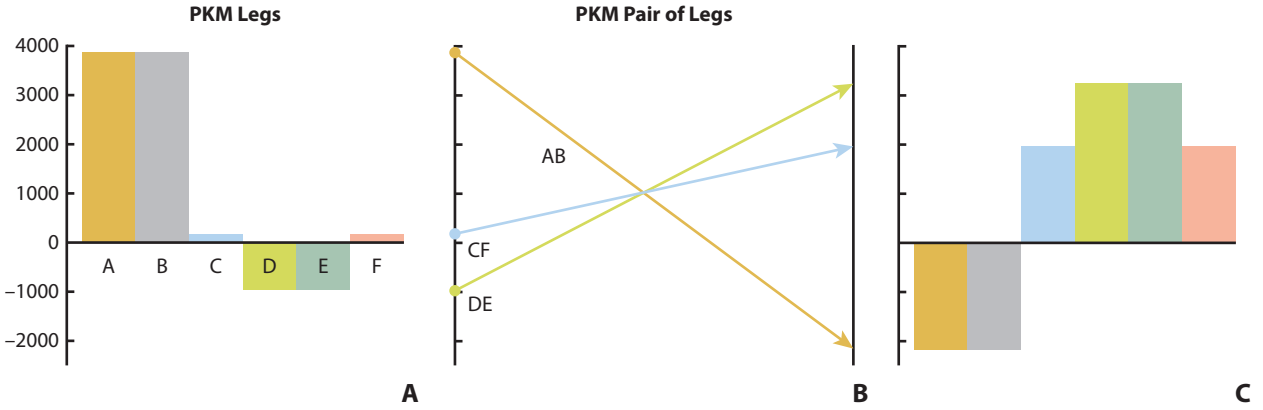

Figure 7. Maximum forces in PKM legs. A, Conforms to case in Figure 6A. B, Represents forces in pair of legs for complete extension of robot. C, Corresponds to case in Figure 6C. PKM, parallel kinematic mechanism.

performed through additional pressure sensors at the hydraulic source and the accumulator, which also helped validate the parametric configuration.

For any patient referred for implant-mandible loading examination, the dental implant module would be set up in 2 parts: a set of metallic pins with capacitive force sensors (Figs. 3, 4) and a patient-specific mandible model with selected sites for load testing (Fig. 5). A single force-sensing element encompassed 5 strain-sensitive thick-film resistors including 1 for linear vertical force and 4 for lateral forces to record the resultant bending moments. The strain was directly affected by the change in pressure during a load-testing cycle. Wheatstone bridges and a simple decoupling amplifier helped record and obtain the respective voltages proportional to the applied forces. Capacitive sensing systems had been successfully adapted as sensorized skin for the whole-body tactile sensing architecture for humanoid robots and robotic hands.[48-51] Similar technologies had been adapted to develop gloves for object handling, especially clothes manipulation.[52,53]

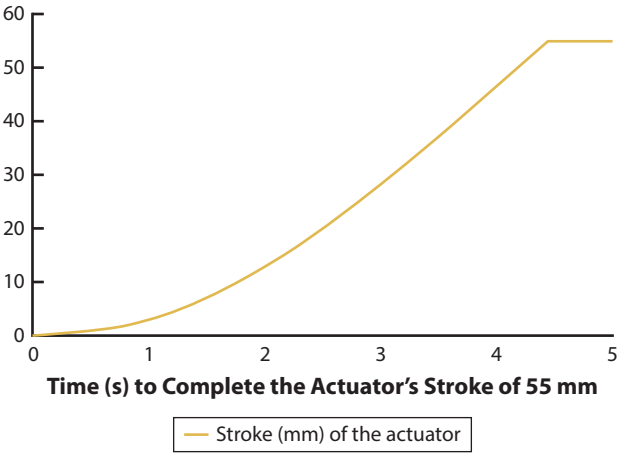

Figure 8. Stroke of hydraulic actuator.

RESULTS

System modeling had verified its capacity to replicate the human mastication with a requisite range of occlusal forces. The relationship between Cartesian forces and

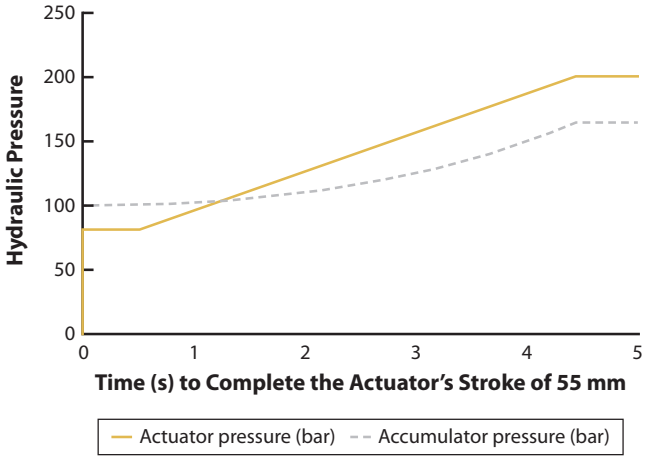

Figure 9. Hydraulic pressure in actuator and accumulator to complete robot extension stroke.

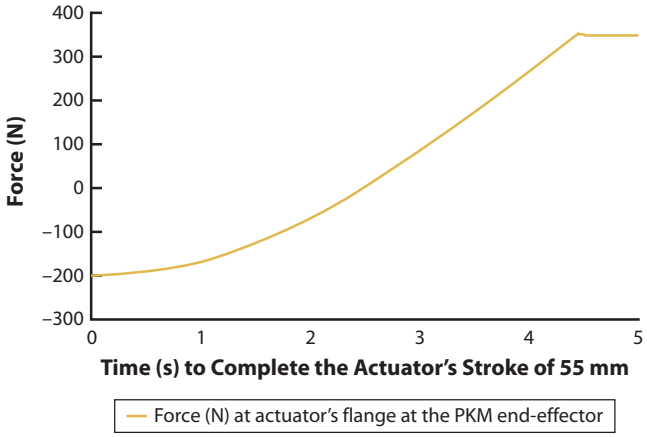

Figure 10. Effective force produced by actuator at PKM end-effector. PKM, parallel kinematic mechanism.

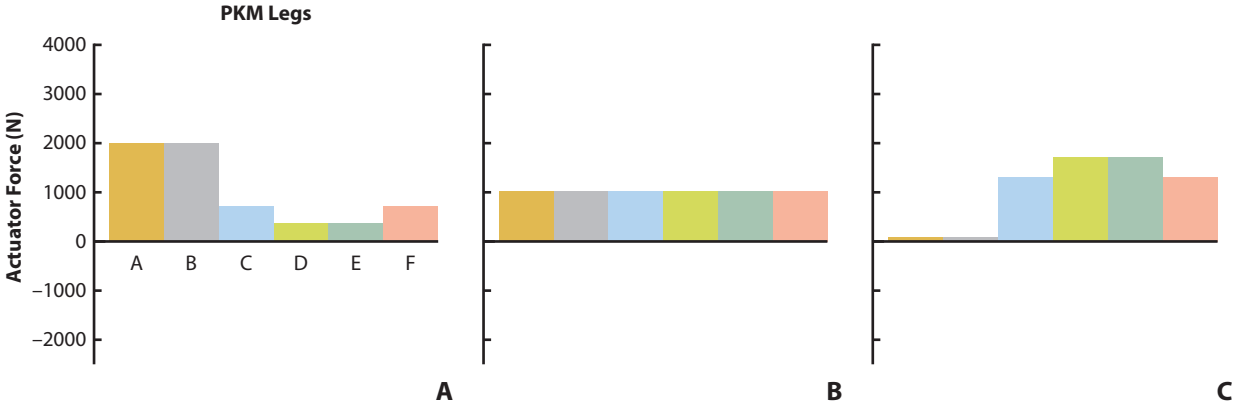

Figure 11. Occlusal replication. Actuator forces during first and second phases of test cycle. A, C, 6-Dof wrench application during second phase. B, Persistent force application by end-effector (no torque) during first phase.

articular forces required parallel structures such as force sensors, as implemented for the current application. The mechanism was plotted for 6 actuators wrench (Fig. 6), validating the required resultant force at the point G on the end-effector as well as the counter moment acting on the end-effector when G was not at the center. The attained forces for PKM legs (Fig. 7) were used for the validation of actuators' design. Hydraulic system modeling verified 3 aspects: legs actuation (Fig. 8), accumulator response (Fig. 9), and output force at the end-effector (Fig. 10). The first stage was accomplished with 1000-N force at the end-effector and G at its center to ensure the parallel interface of the 2 modules. In the second stage, the wrench was executed for the required range of forces (Fig. 11).

For each of the 5 sensing patches in a single load-sensing element, the capacitance was $\Omega = \varepsilon_o(a/\chi)(\delta\chi/\chi)$, where ε_o was the dielectric constant, a was the nominal area of a sensing patch, χ was sensing plates' separation in a sensing patch, and $\delta\chi$ was the strain. With an average variation of $\Delta\Omega = 0.0005$ picofarad(pF), the capacitance range at which the applied sensor operated was 10 $pF < \Omega_o < 20$ pF corresponding to the load measurement for 200 N to 2000 N. The sensor had a fast response rate because of the light inertia of sensing patches, with high sensitivity especially within the required range of mastication forces.

Each test cycle was unique in terms of wrench execution and the test cycle duration based on patient-specific requirements and was performed in 4 steps: dental implant module preparation and attachment to the fixture bridge; PKM operation to engage the end-effector with the dental implant module; mastication cycle execution; and recording of the required load-testing data. To execute a mastication cycle that simulated natural conditions, a fluid bowl was attached at the

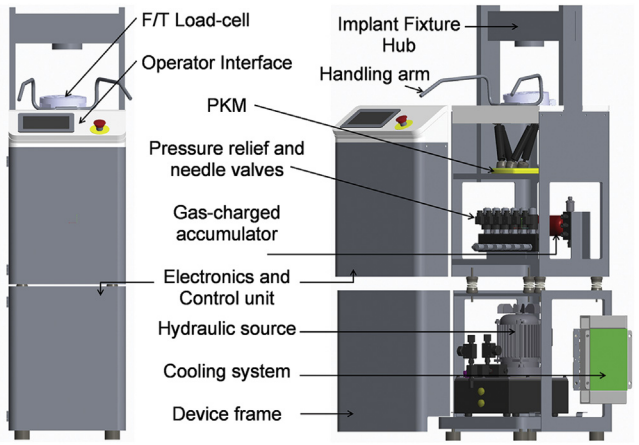

Figure 12. Robotic mastication simulator. Complete hardware architecture.

top of the load cell to keep the dental model submerged in the artificial saliva. Figure 12 described the complete structural design of the apparatus.

DISCUSSION

The focus of the apparatus was multidimensional, realizing an unconventional methodology of executing the robotic mastication and examining the implant-mandible interaction in the form of cost-effective dental laboratory equipment. All the components of the PKM were customized for the realization of this particular application. Spherical floating joints were shaped to accommodate the required skewed orientation of the legs between the base and the end-effector, making the machining process convenient. Similarly, the valves used in the hydraulic circuit had also been tailored to achieve the compactness of the system and an overall economic solution.

This novel apparatus facilitated implementation of the masticatory force cycle dexterously and further facilitated a better imitation of the implant and the mandible interaction that eventually helped record more realistic load-testing data. In contrast with the focus of earlier efforts[28-39] where mandible motion was accomplished by means of manipulators operating an end-effector plate with a focus on its displacement, the current device focused on force transmission between interacting bodies with minimal motion manipulation. However, fluidic compression and joints backlashes during the operational sequence were transformed into impulsive displacements between interacting bodies affecting end-effector stroke, hydraulics operation, and the parameterized configuration. For better performance, these impulsive movements will be compensated mechanically at design level of the PKM along with the implementation of additional sensorization for PKM leg movements. These improvements will further enhance the control of the PKM, serving for better masticatory forces transmission and interactive load data recording.

CONCLUSIONS

Based on modeling and analysis of the design and features of the robotic mastication simulator, the following conclusions were drawn:

1. The PKM effectively implemented the mastication cycle both in terms of Dof and the required level of force execution. Hydraulics of the PKM accomplished the designed load-testing cycle, validating its scheme for the required range of forces and 2-phase operation.
2. The implant-mandible interactive load-sensing element had the capacity to provide smart load recording within the range of mastication forces.
3. The system design exhibited its capacity to facilitate the dental replacement procedure, predicting bone health and implant stability.

REFERENCES

1. Haegele M. Executive summary world robotics 2018 service robots. [document on the Internet]. Frankfurt: IFR Statistical Department; 2018. Available at: https://ifr.org/downloads/press2018/Executive_Summary_WR_Service_Robots_2018.pdf. Accessed January 5, 2019.
2. Dario P, Guglielmelli E, Allotta B, Carrozza MC. Robotics for medical applications. IEEE Robot Autom Mag 1996;3:44-56.
3. Beasley RA. Medical robots: current systems and research directions. J Robot 2012;2012:1-14.
4. Al-Razgan M, Alfallaj LF, Alsarhani NS, Alomair HW. Systematic review of robotics use since 2005. International Journal of Mechanical Engineering and Robotics Research 2016;5:129-32.
5. Tsuda J, Wyatt S, Litzenberger G. World robotics 2018 industrial and service robots. [document on the Internet]. Tokyo: IFR; 2018. Available at:, https://ifr.org/downloads/press2018/WR_Presentation_Industry_and_Service_Robots_rev_5_12_18.pdf. Accessed January 5, 2019.
6. Mirbagheri A, Baniasad MA, Farahmand F, Behzadipour S, Ahmadian A. Medical robotics: state-of-the-art applications and research challenges. Int J Healthc Inf Syst Inform 2013;8:1-4.
7. Rao YV, Parimi AM, Rahul DS, Patel D, Mythreya YN. Robotics in dental implantation. Gupta MS, editor. Materials Today: Proceedings of the International Conference on Advancements in Aeromechanical Materials for Manufacturing (ICAAMM); Jun 26-28, 2016. 4. Hyderabad, India: Elsevier; 2017. p. 9327-32.
8. Kronreif G. Advanced concepts for medical robotic systems. New Horizons in Clin Case Rep 2017;1:5.
9. Otani T, Raigrodski AJ, Mancl L, Kanuma I, Rosen J. In vitro evaluation of accuracy and precision of automated robotic tooth preparation system for porcelain laminate veneers. J Prosthet Dent 2015;114:229-35.
10. Misch CE. Dental implant prosthetics. Hong Kong: Elsevier Health Sciences; 2004. p. 1-31.
11. O'Neill JE, Yeung SC. Do dental implants preserve and maintain alveolar bone? J Investig Clin Dent 2011;2:229-35.
12. Hasan I, Röger B, Heinemann F, Keilig L, Bourauel C. Influence of abutment design on the success of immediately loaded dental implants: experimental and numerical studies. Med Eng Phys 2012;34:817-25.
13. Bicudo P, Reis J, Deus AM, Reis L, Vaz MF. Mechanical behaviour of dental implants. Procedia Struct Integrity 2016;1:26-33.
14. Becker W, Becker BE, Alsuwyed A, Al-Mubarak S. Long-term evaluation of 282 implants in maxillary and mandibular molar positions: a prospective study. J Periodontol 1999;70:896-901.
15. Moy PK, Medina D, Shetty V, Aghaloo TL. Dental implant failure rates and associated risk factors. Int J Oral Maxillofac Implants 2005;20:569-77.
16. Javed F, Romanos GE. The role of primary stability for successful immediate loading of dental implants. A literature review. J Dent 2010;38:612-20.
17. Fuh LJ, Huang HL, Chen CS, Fu KL, Shen YW, Tu MG, et al. Variations in bone density at dental implant sites in different regions of the jawbone. J Oral Rehabil 2010;37:346-51.

18. Boughton OR, Ma S, Zhao S, Arnold M, Lewis A, Hansen U, et al. Measuring bone stiffness using spherical indentation. PLoS One 2018;13:e0200475.
19. Novitskaya E, Chen PY, Hamed E, Jun L, Lubarda VA, Jasiuk I, et al. Recent advances on the measurement and calculation of the elastic moduli of cortical and trabecular bone: a review. Theoret Appl Mech 2011;38:209-97.
20. Shenoy VK, Rodrigue SJ, Prashanti E, Saldanha SJ. Tooth implant supported prosthesis: a literature review. J Interdiscip Dent 2013;3:143-50.
21. Washio K, Tsutsumi Y, Tsumanuma Y, Yano K, Srithanyarat SS, Takagi R, et al. In vivo periodontium formation around titanium implants using periodontal ligament cell sheet. Tissue Eng Part A 2018;24:1273-82.
22. Nooji D, Lunia MR. Tooth-implant supported prostheses - a review. Int J Curr Res 2019;9:50651-6.
23. Lee SH, Bédard O, Buchtová M, Fu K, Richman JM. A new origin for the maxillary jaw. Dev Biol 2004;276:207-24.
24. Xu W, Bronlund JE. Mastication robots: biological inspiration to implementation. Berlin Heidelberg: Springer; 2010. p. 1-285.
25. Kato I, Takanisi A, Asari K, Tani T. Development of artificial mastication system. Construction of one degree of freedom antagonistic muscle model WJ-O. Ann Anat 1988;165:197-203.
26. Takanobu H, Takanishi A, Kato I. Design of a mastication robot mechanism using a human skull model. In: IROS'93: Proceedings of the 1993 EEE/RSJ International Conference on Intelligent Robots and Systems - Intelligent Robots for Flexibility; Jul 26-30, 1993. 3. Yokohama, Japan: IEEE/RSJ; 1993. p. 203-8.
27. Takanobu H, Tanase T, Takanishi A, Kato I. Adaptive masticatory jaw motion using jaw position and biting force information. In: MFI'94: Proceedings of the International Conference on Multisensor Fusion and Integration for Intelligent Systems; Oct 2-5, 1994. Las Vegas: IEEE; 1994. p. 360-5.
28. Takanobu H, Ohtsuki K, Takanishi A, Ohnishi M, Okino A. Jaw training robot and its clinical results. In: AIM 2003: Proceedings of 2003 IEEE/ASME International Conference on Advanced Intelligent Mechatronics; Jul 20-24, 2003. 2. Kobe, Japan: IEEE; 2003. p. 932-7.
29. Okino A, Inoue T, Fujii Y, Nasu T, Takanobu H, Takanishi A, et al. Development of a clinical jaw movement training robot for intermaxillary traction therapy. In: Proceeding of Robotics and Automation; Apr 26-May 1, 2004. 3. New Orleans, Louisiana: ICRA, IEEE; 2004. p. 2492-7.
30. Xu WL, Pap JS, Bronlund J. Design of a biologically inspired parallel robot for foods chewing. IEEE Trans Ind Electron 2008;55:832-41.
31. Xu WL, Torrance JD, Chen BQ, Potgieter J, Bronlund JE, Pap JS. Kinematics and experiments of a life-sized masticatory robot for characterizing food texture. IEEE Trans Ind Electron 2008;55:2121-32.
32. Wang G, Cong M, Xu W, Wen H, Du J. A biomimetic chewing robot of redundantly actuated parallel mechanism. Ind Rob 2015;42:103-9.
33. Sun C, Xu WL, Bronlund JE, Morgenstern M. Dynamics and compliance control of a linkage robot for food chewing. IEEE Trans Ind Electron 2014;61:377-86.
34. Lee SJ, Kim BK, Chun YG, Park DJ. Design of mastication robot with life-sized linear actuator of human muscle and load cells for measuring force distribution on teeth. Mechatronics 2018;51:127-36.
35. Wang L, Sadler JP, Breeding LC. A robotic system for testing dental implants. Mech Mach Theor 1998;33:583-97.
36. Conserva E, Menini M, Tealdo T, Bevilacqua M, Pera F, Ravera G, et al. Robotic chewing simulator for dental materials testing on a sensor-equipped implant setup. Int J Prosthodont 2008;21:501-8.
37. Conserva E, Menini M, Tealdo T, Bevilacqua M, Ravera G, Pera F, et al. The use of a masticatory robot to analyze the shock absorption capacity of different restorative materials for prosthetic implants: a preliminary report. Int J Prosthodont 2009;22:53-5.
38. Alemzadeh K, Hyde RA, Gao J. Prototyping a robotic dental testing simulator. Proc IME H J Eng Med 2007;221:385-96.
39. Raabe D, Alemzadeh K, Harrison AJ, Ireland AJ. The chewing robot: a new biologically-inspired way to evaluate dental restorative materials. In: Engineering the Future of Biomedicine: Proceedings of the 31st Annual International Conference of the IEEE Engineering in Medicine and Biology Society; Sep 3-6, 2009. Minneapolis: IEEE; 2009. p. 6050-3.
40. Machines for the biomedical industry [document on the Internet]. Italy: Italsigma s.r.l. Available at: http://www.italsigma.it/Documents/Italsigma%20brochure%20biomedicale%20-%20eng.pdf. Accessed January 5, 2019.
41. [document on the Internet]Physical property testing equipment for biomaterials and medical applications. Japan: Shimadzu; 2013. Available at:, http://www.shimadzu.com.br/analitica/industrias/biomateriais/catalogos/biomateriais.pdf. Accessed January 5, 2019.
42. Instron dental implant testing - Instron [Internet]. India: Instron. Available at: http://www.instron.in/en-in/testing-solutions/industry-solutions/biomedical/dental/dental-implant-testing. Accessed January 5, 2019.
43. International Organization for Standardization. ISO 14801-2. Dentistry - Implants - Dynamic fatigue test for endosseous dental implants. Switzerland: International Organization for Standardization; 2007. BSOL British Standards Online. Available at: https://bsol.bsigroup.com.
44. International Organization for Standardization. ISO 14801-3. Dentistry - Implants - Dynamic loading test for endosseous dental implants. Switzerland: International Organization for Standardization; 2016. BSOL British Standards Online. Available at: https://bsol.bsigroup.com.
45. Canullo L, Coelho PG, Bonfante EA. Mechanical testing of thin-walled zirconia abutments. J Appl Oral Sci 2013;21:20-4.
46. Toyoshima Y, Wakabayashi N. Load limit of mini-implants with reduced abutment height based on fatigue fracture resistance: experimental and finite element study. Int J Oral Maxillofac Implants 2015;30:e10-6.
47. Bakke M. Bite force and occlusion. Semin Orthod 2006;12:120-6.
48. Schmitz A, Maiolino P, Maggiali M, Natale L, Cannata G, Metta G. Methods and technologies for the implementation of large-scale robot tactile sensors. IEEE Trans Robot 2011;27:389-400.
49. Cannata G, Maggiali M, Metta G, Sandini G. An embedded artificial skin for humanoid robots. In: MFI 2008: Proceeding of the International Conference on Multisensor Fusion and Integration for Intelligent Systems; Aug 20-22, 2008. Seoul, South Korea: IEEE; 2008. p. 434-8.
50. Baglini E, Cannata G, Mastrogiovanni F. Design of an embedded networking infrastructure for whole-body tactile sensing in humanoid robots. In: Humanoids 2008: Proceedings of the 10th IEEE-RAS International Conference on Humanoid Robots; Dec 6-8, 2010. Nashville: IEEE; 2010. p. 671-6.
51. Maiolino P, Maggiali M, Cannata G, Metta G, Natale L. A flexible and robust large scale capacitive tactile system for robots. IEEE Sens J 2013;13:3910-7.
52. Maiolino P, Denei S, Mastrogiovanni F, Cannata G. A sensorized glove for experiments in cloth manipulation. In: RO-MAN 2013: Proceedings of the 22nd IEEE International Symposium on Robot and Human Interactive Communication; Aug 26-29, 2013. Gyeongju, South Korea: IEEE; 2013. p. 336-7.
53. Denei S, Maiolino P, Baglini E, Cannata G. On the development of a tactile sensor for fabric manipulation and classification for industrial applications. In: IROS 2015: Proceedings of the IEEE/RSJ International Conference on Intelligent Robots and Systems; Sep 28-Oct 2, 2015. Hamburg, Germany: IEEE; 2015. p. 5081-6.

Corresponding author:
Dr Ahmad Mahmood Tahir
PMAR Robotics Group
University of Genoa
Via all'Opera PIA 15/A
DIME-PMAR, 16145
Genoa
ITALY
Email: tahir@dimec.unige.it

Acknowledgments
The authors thank Tommaso Lanza, our Graduate Student at the University of Genoa, Genoa, Italy, for his contribution toward hydraulic system modeling of the robotic mastication device.

https://doi.org/10.1016/j.prosdent.2019.06.023